A COMPARATIVE STUDY OF CFD-MODELLING FOR LEAN PREMIXED HYDROGEN DEFLAGRATIONS IN LARGE-SCALE VENTED VESSELS

L. Ivan[1], Z. Liang[1], M. Khalil[2] and C.P.T. Groth[2]

[1]Canadian Nuclear Laboratories, Chalk River, ON, K0J 1J0, Canada, lucian.ivan@cnl.ca
[2]University of Toronto Institute for Aerospace Studies, 4925 Dufferin Street, Toronto, ON, M3H 5T6, Canada, groth@utias.utoronto.ca

ABSTRACT

Hydrogen combustion inside a post-accident nuclear reactor containment may pose a challenge to the containment integrity, which could alter the fission-product release source term to the public. Combustion-generated overpressures may be relieved by venting to adjacent compartments through relief panels or existing openings. Thus, an improved understanding of the propagation of lean hydrogen deflagrations in inter-connected compartments is essential for the development of appropriate management strategies. GOTHIC is a general purpose, lumped parameter thermal-hydraulic code for solving multi-phase compressible flows, which is accepted as an industry-standard code for containment safety analyses. Following the Fukushima accident, the application of three-dimensional computational fluid dynamics methods to high-fidelity detailed analysis of hydrogen combustion processes has become more widespread. In this study, a recently developed large-eddy-simulation (LES) capability is applied to the prediction of lean premixed hydrogen deflagrations in large-scale vented vessels of various configurations. The LES predictions are compared with GOTHIC predictions and experimental data obtained from the large-scale vented combustion test facility at the Canadian Nuclear Laboratories. The LES methodology makes use of a flamelet- or a progress-variable-based combustion model. An empirical burning velocity model is combined with an advanced finite-volume framework and a mesh-independent subfilter-scale model. Descriptions of the LES and GOTHIC modelling approaches used to simulate the hydrogen reactive flows in the vented vessels along with the experimental data sets are given. The potential and limitations of the lumped parameter and LES approaches for accurately describing lean premixed hydrogen deflagrations in vented vessels are discussed.

1.0 INTRODUCTION

During a postulated severe accident in a nuclear power plant, a large amount of hydrogen can be produced from the oxidation of metallic components with water/steam during the in-vessel phase and by molten core concrete interactions during the ex-vessel phase. Hydrogen may migrate into the containment compartments, possibly forming combustible gas mixtures. As evidenced in the Fukushima accident, hydrogen combustion can cause severe damage of the primary and secondary containment structures, resulting in the release of radioactive materials to the environment. Depending on the location of hydrogen release or ignition, combustion-generated overpressures can be relieved by venting to adjacent compartment volumes through relief panels or existing openings. Assessing the integrity of these compartments in the reactor containment building during a postulated severe accident scenario requires a reliable prediction of pressure evolution for vented combustion. As a result, extensive studies on vented combustion were performed at the Canadian Nuclear Laboratories (CNL; formerly Atomic Energy of Canada Limited) using a 6 m^3 sphere [1] and a 120 m^3 rectangular Large-Scale Vented Combustion Test Facility (LSVCTF) [2, 3]. The purpose of these studies was to understand the fundamental mechanisms that govern overpressures resulting from hydrogen deflagration of near lean flamability limit mixtures (6-12 vol.% H_2) that are relevant for accident scenarios. The experimental data was used to develop and validate models used to analyze scenarios in which the deliberate ignition in a post-accident nuclear reactor containment is applied as a mitigation strategy.

In parallel with experimental studies, large efforts were undertaken to validate combustion models and assess computational capabilities [4]. The accurate prediction of the consequences of the combustion process is important for severe accident management. The use of three-dimensional (3D) computational fluid dynamics (CFD) methods has proven useful in this regard, with many organizations and studies adopting such methods to perform detailed simulations of hydrogen release and combustion [5]. However, the routine application of CFD methods to hydrogen

combustion for plant-scale analysis is still hindered by the relatively high computational cost associated with these methods, and therefore, lumped parameter (LP) codes remain widely used for safety analysis [6, 7]. Nevertheless, the validity of either LP or CFD codes needs to be assessed against large-scale experiments representative of severe accident conditions. Furthermore, the advantages and limitations of either approach have to be properly investigated and identified so as to provide guidance on the selection of appropriate computational tools for performing the design and assessment of hydrogen safety measures.

GOTHIC is a general-purpose thermalhydraulics software package, often referred to as CFD-like, that works at length scales in between CFD and LP codes. It is widely used by the nuclear community for safety analysis of containment thermalhydraulics and hydrogen behavior including transport, mixing, and combustion [8]. Alternatively, CFD is a recognized powerful, physics-based modelling and simulation tool that has the potential to provide accurate predictions of large-scale deflagration and transitional combustion processes, such as the deflagration-to-detonation transition (DDT), that are of interest for hydrogen safety. To achieve higher fidelity, CFD simulation frameworks (e.g., [7, 9–12]) rely on sophisticated modelling approaches, such as unsteady Reynolds-averaged Navier-Stokes (URANS) and large-eddy simulation (LES), that not only provide a more accurate description of the turbulence-combustion interaction but also impose certain stringent resolution requirements on the computed solutions. A wide range of length scales must be resolved to simulate large-scale hydrogen deflagrations and therefore, computing requirements for CFD approaches is high. Advance numerical techniques, e.g., high-order accurate methods and solution adaptive meshing, are often required to resolve the flame front and other important features in the computational domain. In contrast, the GOTHIC burning model has a special treatment for flame propagation through coarse meshes. The mesh size is thus independent of the flame front thickness and the computation becomes relatively inexpensive. Compared to CFD codes, the effort required in setting up the GOTHIC input model and the total computational cost are negligibly small, allowing for better scalability to reactor containment applications while still providing more 3D detailed information than purely LP codes do, as shown in the recent work of Lebel and Liang [13]. With that being said, CFD-like codes such as GOTHIC also require that special parametrizations be made in order to treat certain physical phenomena, as they do not have the same level of detail in the treatment of underlying mechanisms.

The focus of this study is to examine the flame dynamics and the associated model considerations for combustion processes in large-scale vented vessels. The primary objective is to assess the performance, potential and limitations of an advanced LES CFD modelling framework and a lumped-parameter, industry-standard code for simulating vented hydrogen deflagrations at the scales typical for practical applications. This is achieved by performing simulations of experiments conducted at the CNL LSVCTF and comparing against the experimentally-observed flame propagation behavior and combustion pressure transients.

2.0 EXPERIMENTAL METHODS

2.1 Testing Facility

The LSVCTF is a 120 m^3 (10 m long, 4 m wide, and 3 m high) rectangular structural steel test chamber enclosed in an insulated Quonset building. The test chamber is constructed of 1.25 cm thick steel plates welded to a rigid steel I-beam framework. The entire structure is anchored to a 1 m thick concrete pad. The end walls are covered with rectangular steel panels bolted to the end-wall structure. The desired venting to the external environment can be achieved by removing the appropriate number of panels from the end wall. Internal walls, made of structural steel beams, can be inserted into the facility to divide the entire chamber into two or three volumes. Eight hydraulic fans are installed in a diagonal pattern on the side walls to mix the gases uniformly during gas addition or to generate turbulence during a test. Figure 1 depicts the test configuration used in this study. The tests presented in this paper were performed in the front chamber (57 m^3) of the LSVCTF by blocking off the vents on the central wall. As shown in Figure 1(b), the front wall had a 0.55 m^2 vent area, consisting of two sections (each with a nominal width of 0.379 m and height of 0.739 m) separated by a 20 cm thick central beam. Prior to the hydrogen addition, the vents were covered with aluminum foil that ruptured at low pressures (i.e., between 1 to 2 kPa) during combustion. Ignition was achieved with a hermetically sealed 120 V TAYCO glow plug igniter. The igniter was located in the center of the front chamber at a height of 1.5 m.

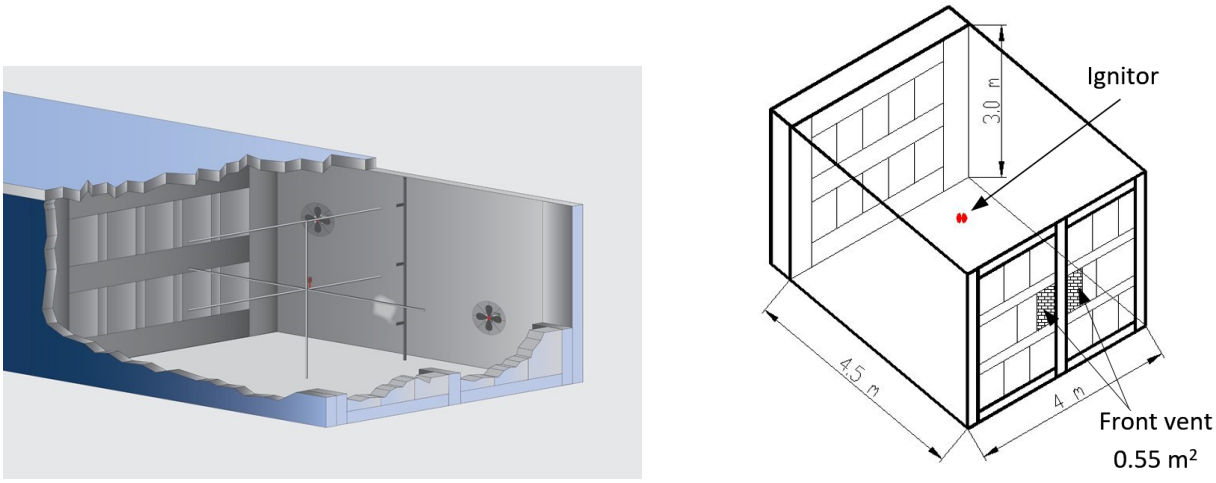

(a) (b)

Figure 1: Schematic of large-scale vented combustion test facility.

2.2 Measurements

The initial gas composition was analyzed by a process mass spectrometer and sampled at 20 s intervals prior to the ignition. The mass spectrometer was calibrated using primary calibration gases of 10 to 30% H_2 by volume in nitrogen. The gas concentrations are always expressed on a volume basis in this paper. The uncertainty was within ±0.2% (absolute).

The transient pressure during combustion was monitored using three Kulite dynamic pressure transducers. The transducers were periodically calibrated with an Ectron pressure calibrator with an overall uncertainty of approximately ±0.5 kPa. The signals of the fast response thermocouples, dynamic pressures and vent rupture voltage were acquired with a high speed data acquisition system at a sampling rate of 1,000 to 5,000 Hz.

2.3 Test Conditions

All tests were performed under ambient conditions (1 atm, ~20–30°C, and ~50% relative humidity or RH). Prior to ignition, all the mixing fans were turned off for quiescent tests, but remained on for turbulent combustion with a fan speed of 1,000 rpm. The ignition was delayed by a minimum of three minutes after the fans were switched off to allow the turbulence field to decay to almost zero intensity for quiescent tests. The maximum air speed was ~9 m/s at the fan locations and ~4 m/s in the center of the room. The volume-averaged turbulent fluctuation velocity was on the order of 1 m/s. For the present study, the experimental tests FC009 and FC0807 were used to perform a preliminary comparison between the two modelling approaches considered. For FC009, the test conditions of a 10% hydrogen concentration and fan settings set to quiescent conditions lead to a measured maximum overpressure of 12.5 kPa. In contrast, the FC0807 case corresponds to turbulent conditions and a 9% hydrogen concentration, which lead to a maximum measured overpressure of approximately 35 kPa.

3.0 MODELLING WITH LUMPED PARAMETERS

3.1 GOTHIC Model

GOTHIC code solves the conservation equations for mass, momentum and energy for multicomponent, multiphase compressible flow in lumped (single node) parameter and/or multi-dimensional geometries, or any combination of these within a single model. The balance equations are coupled by mechanistic models for interface mass, momentum, and energy transfer [14]. Figure 2 shows the GOTHIC model layout and the nodalisation used in this work. The front chamber is represented by the control volume "2s", which has nominal dimensions of 4.5 m long, 4.0 m wide, and 3.0 m tall in each Cartesian x-, y-, and z-direction, respectively. Depending on the venting area of the test, the front chamber is subdivided with a 3D Cartesian mesh consisting of $10 \times 11 \times 8$ control volumes in the case of a venting area of 0.55 m^2 and, similarly, $10 \times 13 \times 8$ volumes in the case of a venting area of 0.35

m^2. Thus, the resulting mesh spacing in each Cartesian direction is $\Delta x = 0.450$ m, Δy varying between 0.2 and 0.38 m, and $\Delta z = 0.375$ m. The grid nodes along the y-and z-axis accommodate the location of the front vents. The external atmosphere was modelled with a large lumped-parameter volume (control volume 1 in Figure 2) having the pressure regulated by a pressure boundary condition. The front vents were modelled using GOTHIC's built-in flow connectors, through which the adjacent cells in control volumes 1 and 2s are hydraulically connected. A quick-open valve was applied to the connectors with a user-defined OPEN trip to control the vent opening. The vent rupture pressure was set at 1.5 kPa higher than the ambient pressure, p_{amb} = 101.325 kPa. The heat transfer between the fluid and the vessel ceiling was simulated as follows. All instances of conduction were modelled as one-dimensional and perpendicular to the structure surface. The inside surface of the ceiling was assumed to have a heat transfer coefficient of 200 W/m^2-K and the external surface was assumed to be perfectly insulated (i.e., zero heat transfer coefficient). The heat loss to the other walls was neglected because the burnt gas is mostly in contact with the ceiling. The use of this heat transfer model was found to lead to the best agreement with the measured pressure in previous GOTHIC combustion modeling of LSVCTF experiments.

The default GOTHIC modelling options for mass and heat transfer (including condensation) were used in the present work, and the standard two-equation $k-\epsilon$ model was used to account for the presence of turbulence. Although no grid convergence studies were carried out in the present study, the choice of grid discretization and modelling options is considered adequate based on past experience with GOTHIC combustion modeling [13] and proprietary studies for LSVCTF experiments. In these earlier grid sensitivity studies performed for multiple test conditions, it was found that despite capturing more spatial details with finer resolution grids the pressure increase generated by the combustion process was mostly insensitive to the cell count used for the discretization of the combustion chamber.

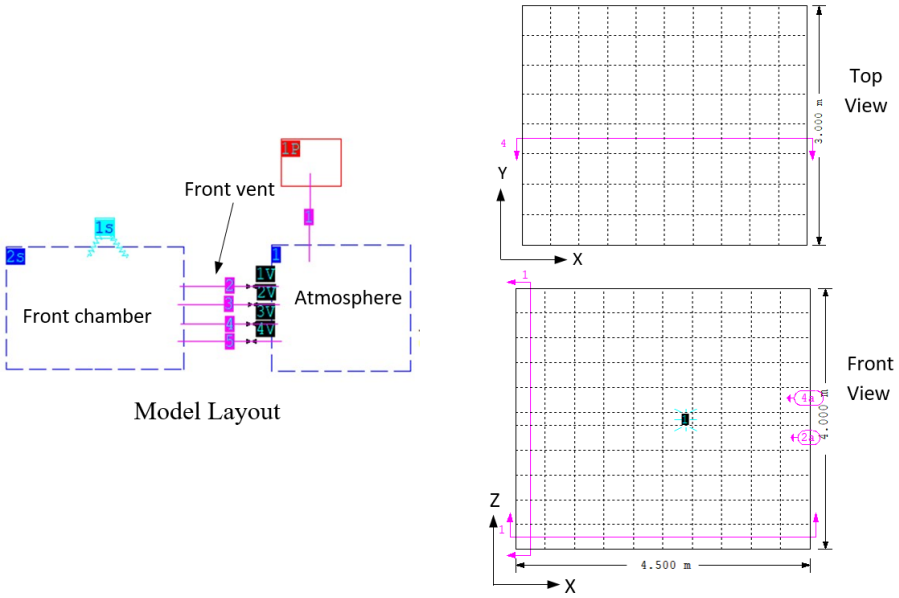

Figure 2: Schematic of GOTHIC model layout (left) and subdivision into control volumes for the front chamber (right) used for modelling the vented combustion in LSVCTF with LP. The front chamber and the external atmosphere control volumes are labeled 2s and 1, respectively. The figure also shows the flow paths for the vents (1V to 4V), the atmospheric pressure boundary (1P), and the heat transfer boundary (1s).

3.2 Combustion Model

GOTHIC's mechanistic burn model [14] was used to simulate combustion in this work. In this model, combustion of hydrogen, which is highly dependent on local hydrogen and oxygen concentrations and turbulence levels, is continuously calculated in a control volume once the mixture composition satisfies the user-defined flammability limits. The combustion rate is determined from the maximum of the laminar, ω_L, and turbulent burning rates, ω_T. The former is defined as a function of laminar flame speed, s_L, and the latter is calculated using the wrinkled

laminar flame model, which assumes the increase in burning rate due to turbulence is proportional to the amount of wrinkle along the reaction front, according to the equation

$$\omega_{\mathrm{T}} = \frac{(s_{\mathrm{L}}\Theta + k^{0.5})\rho_H}{\delta_{ff}}\,, \tag{1}$$

where Θ is a user-defined burn enhancement factor applied as a forcing function to the laminar burning velocity (see more details in Section 3.3), ρ_H is the effective hydrogen density, and δ_{ff} is the flame front thickness parameter. The amount of wrinkle is assumed to be proportional to the root-mean-square of the turbulent kinetic energy, k, in the flow field. The advantage of the "wrinkled laminar flame model" is that it minimizes the dependence of the overall burning rate on the mesh size. This is particularly important for the simulation of containment buildings because of the computational cost. As shown in Section 3.0, the computational cell size of the GOTHIC model is on the order of 10^{-1} m, which is several orders of magnitude larger than the flame thickness which is several millimeters or less. The combustion rate within a computational cell, $\dot{m}_H$, is given by the product of the turbulent burning rate (Equation 1) and the effective burn volume within the cell, V_{eff},

$$\dot{m}_H = \omega_{\mathrm{T}} V_{eff} = (s_{\mathrm{L}}\Theta + k^{0.5})\rho_H A_{ff}\,. \tag{2}$$

In Equation 2, the flame front thickness parameter, δ_{ff}, cancels out by considering that the effective burn volume depends on the flame front thickness parameter and flame front area, A_{ff}, which in turn is estimated based on the area of the cell that is normal to the direction of the hydrogen concentration gradient.

The effective hydrogen density is weighted by the density in the cell where ignition occurs as well as by the density in adjacent cells. This procedure, combined with the effective volume, allows the flame to propagate through coarse computational cells at a nearly constant rate. The laminar flame speed correlation used in the GOTHIC code for hydrogen concentrations less than 15% in air under ambient conditions is a curve fit of CNL experimental data [14] which uses an effective hydrogen concentration determined by the hydrogen concentration in the ignition cell as well as the concentration in the neighboring cells. A similar treatment is also applied to the fluid temperature as numerical diffusion tends to flatten the temperature profile given the large computational cells and thus, the flame front may not propagate at a realistic rate. To alleviate this problem, an effective gas temperature, based on that of the ignition cell and the adjacent cells, is used to control the flame propagation speed. Ignition of hydrogen is activated by an igniter component that was switched on at the beginning of the simulation and turned off after 0.5 s. This procedure provides a high effective temperature to initiate a high rate of chemical reactions inside the ignition cell.

3.3 Burn Enhancement Factor

The abundance and complexity of the mechanisms controlling flame acceleration makes modeling of the pressure history very challenging. Simplifications and empiricism are required. Turbulence induced by venting has been recognized as a significant factor for burn enhancement. Molkov *et al.* [6] performed simulations of experiments performed by Kumar *et al.* [1] with H_2-air mixtures in a 2.3 m-diameter sphere. The predicted pressure transient presented good agreement with the experimental measurements when the burn enhancement factor was in the range $\chi = 1.45 - 2.15$ for 10 and 20% H_2-air mixtures. Other researchers also successfully implemented and used this methodology for simulations of vented deflagrations despite limitations in capturing the actual underlying physics. Solberg *et al.* [15] recommended a burn enhancement factor range of 2.0-2.5 for spherical vessels and hydrogen carbon-air mixtures. Rasbash *et al.* [16] also suggested a burn enhancement factor of 2.0 for quiescent hydrocarbon-air mixtures. The same methodology was also used by Chippett [17] to account for any initial stirring or movement to the gas mixtures (i.e., fan-induced initial turbulence). In GOTHIC, this is taken into account through the application of the burn enhancement factor, Θ, on the laminar flame speed, as shown in Equation 1. In the present study, a global burn enhancement factor is applied to all control volumes in the system and maintained constant during the combustion. The use of multiple factors for different compartments and combustion stages is a subject of future study. For quiescent test conditions such as the case FC009, a burn enhancement factor of 2.5 is applied. For turbulent test conditions, the burn enhancement factors was estimated based on the ratio of the turbulence fluctuation velocity and the laminar flame speed. In particular, $\Theta = 6.1$ for FC0807 case.

4.0 LES COMBUSTION MODELLING AND GOVERNING EQUATIONS

The LES modelling approach adopted herein is based on the framework developed and applied successfully in previous LES studies of premixed flames by Hernandez-Perez *et al.* [18, 19] and Shahbazian *et al.* [20]. More recently, Taylor *et al.* [9] have extended the formulation to hydrogen premixed mixtures and performed studies in closed vessels. This section provides a brief summary of the LES formulation, the computational framework, and the setup of the vented vessel model used in the present study.

4.1 Favre-Filtered Governing Equations

The Favre-filtered form of the Navier-Stokes equations governing compressible flows of a thermally perfect reactive gaseous mixture is used herein to describe the turbulent premixed combustion processes. The Dufour, Soret and radiation effects are neglected. The transport equations for the mixture mass, momentum, energy, and species concentrations can be written as

$$\frac{\partial \overline{\rho}}{\partial t} + \frac{\partial \left(\overline{\rho}\tilde{u}_j\right)}{\partial x_j} = 0\,, \tag{3a}$$

$$\frac{\partial \left(\overline{\rho}\tilde{u}_i\right)}{\partial t} + \frac{\partial \left(\overline{\rho}\tilde{u}_i\tilde{u}_j + \delta_{ij}\overline{p} - \check{\tau}_{ij}\right)}{\partial x_j} = \overline{\rho}g_i - \frac{\partial \sigma_{ij}}{\partial x_j}\,, \tag{3b}$$

$$\begin{aligned}\frac{\partial \left(\overline{\rho}\tilde{E}\right)}{\partial t} + \frac{\partial \left[\left(\overline{\rho}\tilde{E} + \overline{p}\right)\tilde{u}_j + \check{q}_j\right]}{\partial x_j} - \frac{\partial \left(\check{\tau}_{ij}\tilde{u}_i\right)}{\partial x_j} &= \overline{\rho}\tilde{u}_j g_j - \frac{\partial \left[\overline{\rho}\left(\widetilde{h_s u_j} - \tilde{h}_s\tilde{u}_j\right)\right]}{\partial x_j} - \frac{1}{2}\frac{\partial \left[\overline{\rho}\left(\widetilde{u_j u_i u_i} - \tilde{u}_j\tilde{u}_i\tilde{u}_i\right)\right]}{\partial x_j} \\ &\quad - \frac{\partial}{\partial x_j}\left[\Sigma_{n=1}^{N_s}\Delta h^0_{f,n}\overline{\rho}\left(\widetilde{Y_n u_j} - \tilde{Y}_n\tilde{u}_j\right)\right]\,,\end{aligned} \tag{3c}$$

$$\frac{\partial \left(\overline{\rho}\tilde{Y}_n\right)}{\partial t} + \frac{\partial \left(\overline{\rho}\tilde{Y}_n\tilde{u}_j\right)}{\partial x_j} + \frac{\partial \check{\jmath}_{n,j}}{\partial x_j} = \overline{\dot{\omega}}_n + \frac{\partial \left[\overline{\rho}\left(\widetilde{Y_n u_j} - \tilde{Y}_n\tilde{u}_j\right)\right]}{\partial x_j}\,, \tag{3d}$$

where an overbar "-" represents a filtered quantity, a tilde "~" represents a Favre-filtered quantity, and a chevron "ˇ" represents a quantity evaluated in terms of filtered quantities. In Equation 3a-3d, ρ is the mixture density, u_i is the mixture velocity vector, p is the pressure, τ_{ij} is the fluid stress tensor, g_i is the acceleration vector due to gravity, E is the total energy of the mixture, q_i is the heat flux vector, and Y_n, $\jmath_{n,j}$ and $\dot{\omega}_n$ are the mass fraction, the mass flux relative to the mixture, and the reaction rate for species n, respectively. Additionally, $\sigma_{ij} = \overline{\rho}(\widetilde{u_i u_j} - \tilde{u}_i\tilde{u}_j)$ is the SFS stress tensor, h_s is the sensible enthalpy, $\Delta h^0_{f,n}$ is the heat of formation for species n, and δ_{ij} is the Kronecker delta function. Modelling of the LES SFS stress tensor, σ_{ij}, and a number of the other high-order correlations appearing above is required for closure of this filtered equation set. In the expressions above, Einstein summation convention applies to the indices i and j.

4.2 Sub-Filter Scale Modelling

The Integral Length Scale Approximation (ILSA) model [21, 22] is used herein to evaluate the SFS stress tensor, σ_{ij}. Following an eddy viscosity approach, the stress tensor takes the form

$$\sigma_{ij} - \frac{\delta_{ij}}{3}\sigma_{kk} = -2\overline{\rho}\nu_{\mathrm{SFS}}(\check{S}_{ij} - \frac{\delta_{ij}}{3}\check{S}_{kk})\,, \tag{4}$$

where $\check{S}_{ij}$ is the resolved rate of strain tensor and ν_{SFS} is the SFS turbulent viscosity. The ILSA model was developed specifically as a mesh independent SFS LES model, which makes it suitable for use in conjunction with non-uniform meshes such as those obtained through the application of an adaptive mesh refinement procedure [9]. The turbulent viscosity in Equation 4 is defined as [22]

$$\nu_{\mathrm{SFS}} = (C_k L_{\mathrm{est}})^2|\check{S}|\,, \tag{5}$$

where C_k is a model coefficient and L_{est} is the estimated integral length scale of the turbulence. Both of these are calculated using the local averaged resolved flow quantities; the estimated integral length scale is calculated using

$$L_{\mathrm{est}} = \frac{\langle K_{\mathrm{res}}\rangle^{3/2}}{\langle \varepsilon_{\mathrm{tot}}\rangle}\,, \tag{6}$$

where K_{res} is the resolved turbulent kinetic energy and ε_{tot} is the total (resolved and SFS) turbulent dissipation. Angled brackets represent averaged quantities, either spatially over homogeneous planes or directions, or temporally where no spatial homogeneity exists. Since no homogeneous spatial directions are expected for the present closed vessel simulations, temporal averaging was used herein to find the averaged quantities. The model coefficient, C_k, is found by solving locally a quartic equation and its value is dependent on a target level for the modelled turbulence relative to the total. Thus, the ILSA model remains active even as the mesh is refined. Following previous work [18–20], standard gradient transport assumptions are used to determine the SFS scalar enthalpy and species fluxes in terms of the SFS eddy viscosity and SFS turbulent Prandtl and Schmidt numbers.

4.3 Flamelet-Based Combustion Model

To model the interaction between the chemical kinetics and turbulence and to specify the filtered reaction rates for the premixed flame of interest here, a standard flamelet-based combustion model is applied. In this approach, rather than solving directly for the species mass fractions, a reaction progress variable, c, is introduced based on the mass fraction of the fuel in the burned and unburned states ($c \in [0, 1]$). Thus, $c = 0$ corresponds to a mixture of fresh (pure) reactants and $c = 1$ to a mixture of burnt products. The treatment of the chemical kinetics is then reduced to solving a single filtered transport equation for the reaction progress variable, which takes the form [20]

$$\begin{aligned} \frac{\partial}{\partial t}(\overline{\rho}\tilde{c}) + \frac{\partial}{\partial x_j}(\overline{\rho}\tilde{c}\tilde{u}_j) + \frac{\partial}{\partial x_j}[\overline{\rho}(\widetilde{u_j c} - \tilde{u}_j\tilde{c})] &= \rho_u s_T |\nabla\tilde{c}| \\ &= \rho_u s_L \Xi_\Delta |\nabla\tilde{c}| + S_{ign}, \end{aligned} \tag{7}$$

where ρ_u is the density of the reactants, s_T is the modelled turbulent flame speed, $\rho_u s_L \Xi_\Delta |\nabla\tilde{c}|$ is the overall burning rate, and S_{ign} is an empirically-based forcing term to represent the unsteady ignition of the premixed fuel and air by an external igniter. For the vented deflagrations considered herein, the forcing term drives the value of the progress variable in a small volume of the domain to a fully burned state for a specified period of time. More specifically, S_{ign} has the form of a Gaussian spatial shape with the peak at the ignition location, $\vec{x}_{ign}$, and a squared standard deviation of 0.00(2), and a relaxation type amplitude that limit the temporal duration of the ignition term up to $\tau_{ign} = 0.02$ ms.

Combustion pressure in a vented volume is influenced by the rate of heat release due to combustion and the rate of mass loss due to venting. While the latter depends on the vent size and the pressure differential across the vent opening, the former depends on a number of processes that are affected by the scale of the experimental set up. The empirical-based burning velocity model (BVM) of Morkov and Bragin [23] is applied here to determine the combined filtered chemical reaction rate for the progress variable. The turbulent flame speed, $s_T = s_L \Xi_\Delta$ (see Equation 7), is evaluated by applying a multiplicative factor, Ξ_Δ, to the laminar flame speed s_L. This accounts for flame wrinkling, thermodiffusive, and initial turbulence effects (see [7, 23] for details). The laminar flame speed of hydrogen-air-steam mixtures is determined herein *a priori* for a range of concentrations/equivalence ratios by using the Cantera software package [24] in conjunction with the chemical mechanism of Alekseev *et al.* [25] which involves 9 chemical species and 20 reactions. The laminar flame speed was tabulated over a range of pressures which spanned the pressure conditions within the vessel during the combustion process. LES simulations used laminar flame speed values interpolated assuming isentropic compression.

4.4 Solution Procedure for Solving LES Governing Equations

The solution procedure developed by Hernandez-Perez *et al.* [18, 19], Shahbazian *et al.* [20] and Taylor *et al.* [9], and the implementation provided in the in-house CFD code called CFFC (Computational Framework for Fluids and Combustion) represent the computational framework used in this work. The governing LES equations for reacting flow outlined above are solved by applying a finite-volume spatial discretization procedure to each computational cell of a 3D multi-block body-fitted mesh composed of hexahedral volume elements. The finite-volume scheme makes use of a piecewise limited linear solution reconstruction and Riemann solver-based flux functions in the evaluation of the inviscid solution fluxes and, for the viscous fluxes, a centrally-weighted scheme is adopted. For this study, the slope limiter of van Leer [26] and the approximate Roe Riemann solver [27] are used in the inviscid flux evaluation. A standard second-order Runge-Kutta explicit time marching scheme is used to integrate the non-linear system of first-order ordinary differential equations resulting from the finite-volume discretization procedure and evolve the solution within each computational cell forward in time.

4.5 Computational Model and Simulation Setup

To perform LES simulations of hydrogen deflagrations in the half-chamber, double vent LSVCTF configuration described above, a multi-block meshing tool allowing a variable number of blocks was developed for this geometry with representations of the following subdomains: 1) a combustion chamber with the hydrogen-air mixture and igniter having dimensions 4.5×4.0×3.0 m (see Figure 1(b)), 2) the vent domain with a 0.5 m length representing the vent geometry and exit plane for the release, and 3) the exterior domain defining the external environment to the vessel, which is taken as a cuboid of 10 m length, 10 m width and 6 m height for the cases included herein.

Although the CFFC code features a flexible block-based anisotropic mesh adaption strategy on body-fitted multi-block mesh, the results included in this work have been obtained on a mesh similar to the one shown in Figure 3. In particular, a non-adapted, computational multi-block grid has been generated which has 476, 12×12×10, blocks for a total of 685,440 hexahedral computational cells. The mesh spacing in the combustion chamber in the lengthwise direction is constant and equal to 0.018 m. Due to the presence of the vents, the mesh spacing in the widthwise direction varies between 0.016 m, at the center, and 0.124 m, near the wall. Similarly, the mesh spacing in the height direction was between 0.060 m to 0.096 m. The venting domain and the exterior environment were discretized similarly to the depiction in Figure 3(b), which provided a comparable lengthwise mesh resolution along the vents and near the exit plane to the exterior environment with that used for the combustion chamber.

For the present numerical study, the combustion chamber and vent walls were assumed to be perfectly insulated, whereas fixed pressure subsonic outflow boundary conditions were imposed to the frontiers of the exterior environment. The mesh was designed to alter the vent boundary conditions during the course of a simulation to emulate the vent diaphragm rupture and vent opening as a function of pressure that occurs in the experiments. The simulations were initialized at standard atmospheric conditions with an isotropic homogeneous turbulent flow with intensity, u_{rms} (root-mean-square average turbulence velocity), using the procedure of Rogallo [28]. For FC009 and FC0807 conditions, the resulting turbulence intensity as set by the initial turbulent kinetic energy per unit mass (TKE) on the grid is $u_{\text{rms}} = 0.365$ and $u_{\text{rms}} = 2.907$, respectively.

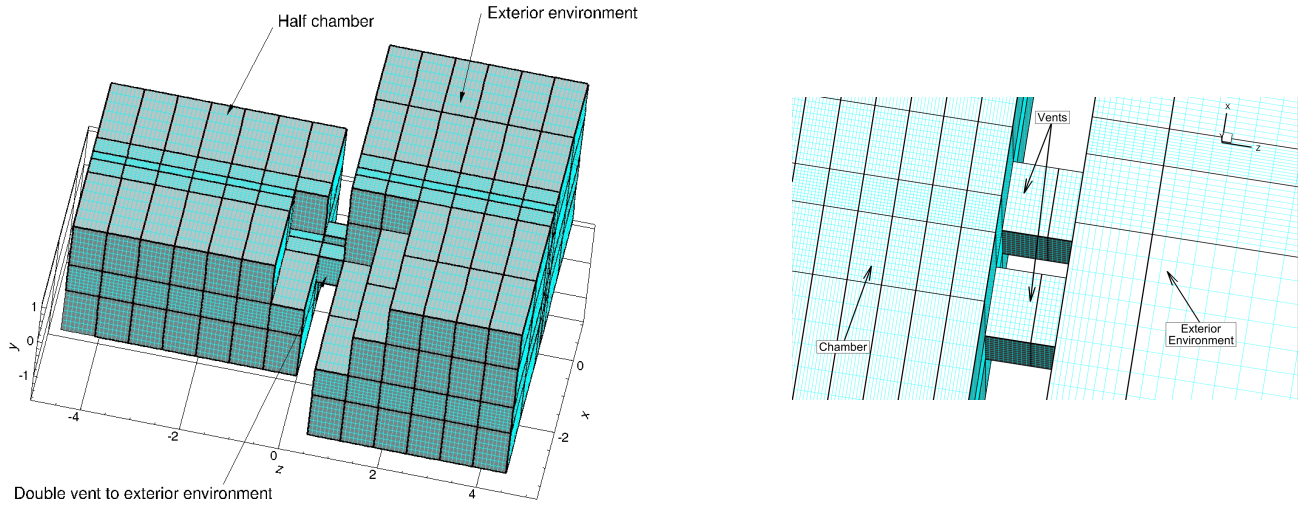

(a) Illustration of a grid with regular (i.e., not stretched) lengthwise mesh spacing.

(b) Detail view near the venting channels showing a lengthwise-stretched grid mesh for the outside environment.

Figure 3: Example of computational domain for solving the LES model with the CFFC code for half-chamber test cases. The main geometric elements, i.e., the combustion chamber, venting channels, and outside environment are identified. The block boundaries of the multi-block structured grid are depicted with thick lines whereas thin lines identify computational cell boundaries.

5.0 SIMULATION RESULTS AND DISCUSSION

Results obtained for both LP (GOTHIC code) and LES (CFFC code) CFD-modelling approaches are included herein for the cases FC009 and FC0807 described in Section 2.3. For the quiescent case, FC009, Figure 4 provides the

predicted time histories of the overpressure inside the vessel by both LP and LES models along with the LSVCTF experimental data collected by pressure transducers located on the vessel wall. Relevant peaks for each pressure history shown in Figure 4 are identified and marked with the same colour as that of the corresponding curve. The underlying physics of each peak occuring in vented combustion is explained in detail in [2, 7]. The first overpressure peak, P1, occurs immediately after the vent diaphragm ruptures which leads to unburned mixture escaping the vessel. Both LP and LES results capture quite accurately the peak magnitude, which is rather expected, but the peak overpressure experiences an earlier onset of about 0.15 s in the LP result when compared to experiment, which is indicative of a faster burning rate in the combustion model and is likely a direct consequence of using a constant burn enhancement factor throughout the simulation. Although the occurrence of P1 is also predicted earlier by the LES simulation, the predicted pressure is in greater agreement with the experimental data for the transition to the first peak. The second peak, P2, occurs when the distorted flame front reaches the vent opening, allowing the burnt gases to be expelled from the vessel and burning to occur externally. In the experiments, this pressure peak is clearly observed, but in the numerical simulations only a slight slope change is noticed for both LP and LES models due to an already high burning rate which compensates through thermal expansion for the hot gases leaving the vessel. Thus, for the LP and LES simulations, P2 is identified based on the flame shape shown in Figures 5 and 6, respectively, and discussed below. Further inspection of Figure 4 shows that the LP model predicts the minimum pressure encountered after the vent opens quite accurately, but the time interval to recover the lost pressure, which is determined experimentally to occur at around the 1.7 s mark, is excessively underestimated. Although the onset of the maximum overpressure peak, P3, predicted by the LP model is also underestimated (occurring at around 1.1 s versus 2.4 s experimentally), the period of time for which the pressure rise and decay is primarily driven by high-frequency thermo-acoustic coupling is matched relatively well by the LP model. The maximum encountered overpressure is overestimated by 16% relative to the smoothed experimental curve. In the case of the LES result, despite a slight overestimate of the pressure decrease following the first peak, the predicted pressure increase towards the second peak, P2, is more accurate. Although the instance at which the maximum overpressure occurs is better estimated than that provided by the LP model, yet still significantly underestimated relative to the smoothed experimental curve, the maximum overpressure is underestimated by 32%. Note that whereas the peak P3 can be clearly identified in the experimental data by the presence of high-frequency thermo-acoustic coupling which leads to flame acceleration and a maximum overpressure [2], the corresponding peaks in the numerical simulations are rather associated with the flame front reaching the vessel walls and the development of a maximum flame front.

To gain more insight into the predictive capabilities of the two model approaches considered, it is valuable to analyze the predicted temperature distribution in the vented vessel in correlation to the pressure history shown in Figure 4. Figure 5 and 6 show three time instances relevant to the transition history of the predicted solution by the LP and LES model, respectively. The solution corresponding to the first time instance in both figures is a snapshot captured around the time the vents opened. The LP result in Figure 5(a) shows a fairly symmetric flame in all directions, whereas the LES solution in Figure 6(a) is clearly distorted and shifted upwards which is due to the buoyancy of the hot gases. Following the opening of the vents, the flame gets stretched to the right which is towards the vent wall. Although the LP model captures this flame stretching, the upwards motion of the hot gases due to buoyancy cannot be observed at this stage. Figure 6(b) and (c) show that the flame front predicted by the LES model advances mostly towards the chamber ceiling and the exit plane for the release, a behaviour consistent with experimental observations [2]. Finally, Figure 5(c) and Figure 6(c) illustrate that before the maximum pressure is attained the flame front reached almost the entire unburned mixture in the vented vessel.

Finally, Figure 7 shows the predicted time histories of overpressure inside the chamber for the LP and LES models for the conditions corresponding to the case FC0807. Relative to the reference time t=0.5 s, the vent opens after 0.22 s which is well predicted by the LES model. The LP model predicts an earlier onset for this peak. The LES pressure history is in great agreement with the experimental data until the occurrence of the second peak. In this turbulent case, the burning rate is increased by the higher levels of turbulence as is the pressure rise occurring after the second peak. Overall, the LP model prediction agrees better with the experimental data than the LES solution. Numerical and other modelling parameter choices may explain this behaviour, which is currently under investigation.

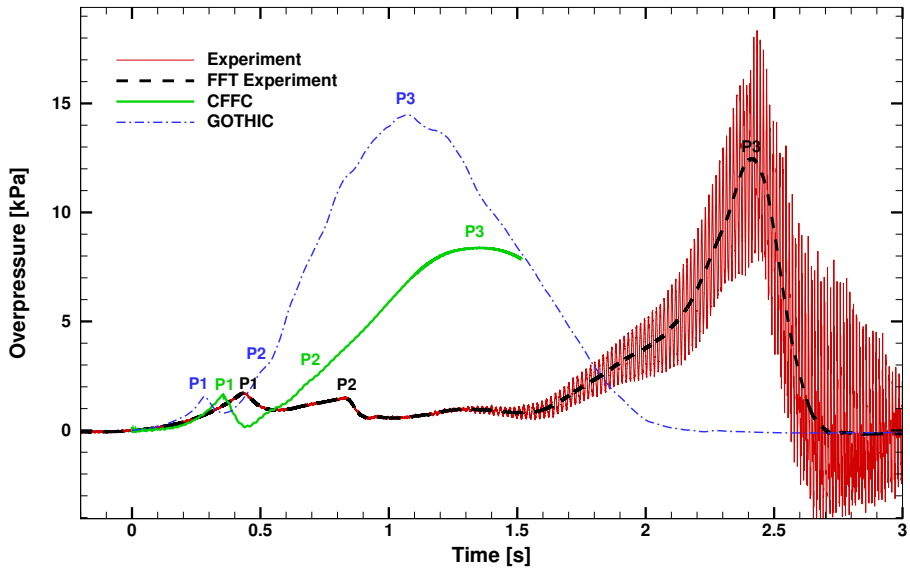

Figure 4: Predicted time histories of the vessel overpressure by the LP and LES models for the half-chamber case with 10% hydrogen fuel-air mixture and quiescent turbulence conditions. The pressure transients are compared to the LSVCTF measurements and a curved obtained by smoothing with Fast Fourier Transform (see [2] for details).

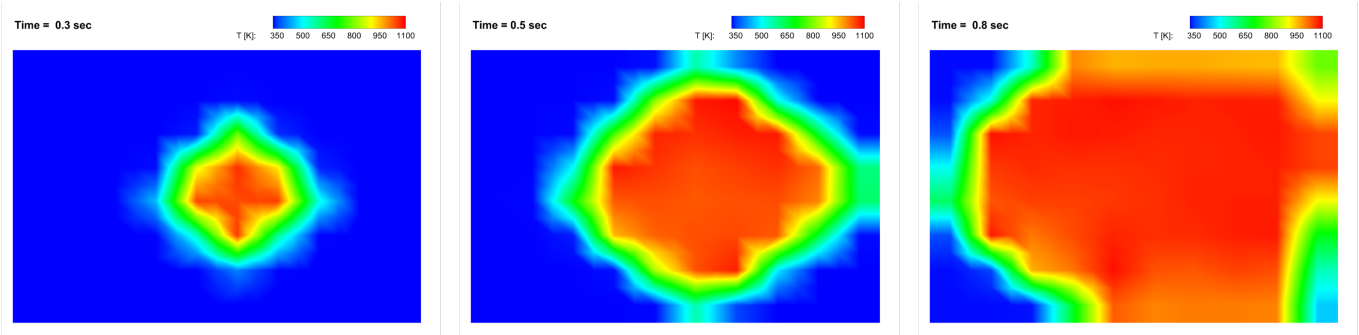

(a) (b) (c)

Figure 5: Predicted temperature distribution by the LP model (GOTHIC code) for three time instances. The vents are located on the right boundary. Figure (a) shows the solution soon after the vents opened, as indicated by the pressure history shown in Figure 4. Figure (b) and (c) illustrate the solution as the flame reaches the vent wall and engulfs most of the chamber, respectively.

6.0 CONCLUSIONS AND FUTURE WORK

Lumped parameter and LES predictions of lean premixed hydrogen deflagrations in vented vessels have been presented and compared to available experimental data from the LSVCTF of CNL. The LP CFD-like GOTHIC code represents an industry-standard code for containment safety analyses. The LES method implemented in the CFFC code makes use of a combination of progress-variable flamelet and BVM models for describing the turbulent burning and propagation of the premixed hydrogen flames and the ILSA SFS model for treatment of the unresolved turbulence. A finite-volume-based computational framework was used to solve the governing LES equations. Although this preliminary study demonstrate a strong potential of the proposed LES approach for accurately describing the physics associated with lean premixed hydrogen deflagrations in vented vessels, it remains to determine how to best exploit any gained accuracy over lumped parameter solvers for routine safety analyses, which comes at the expense of a significantly higher computational cost. The next steps would include utilizing advanced numerical techniques such as the anisotropic, block-based AMR to refine the mesh for the purpose of obtaining a more detailed solution at a reduced computational cost, and also for capturing the acoustic coupling responsible for driving the overpressure in the quiescent cases. The extension of the study to include additional tests configurations from the LSVCTF are considered for follow-on studies.

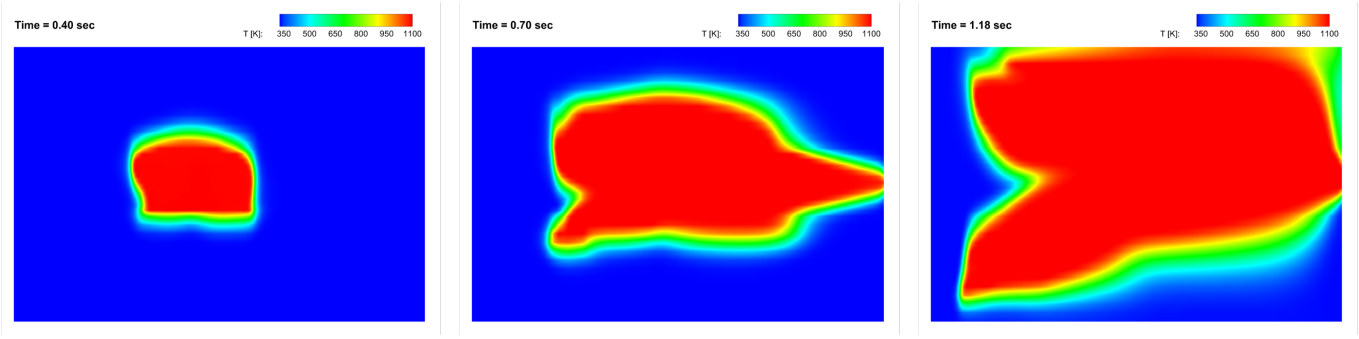

(a) (b) (c)

Figure 6: Predicted temperature distribution with the LES model (CFFC code) for three time instances. The vents are located on the right boundary. Figure (a) shows the solution soon after the vents are opened (see the pressure history in Figure 4). In (b) and (c) the flame front reached the vent wall and chamber ceiling, respectively.

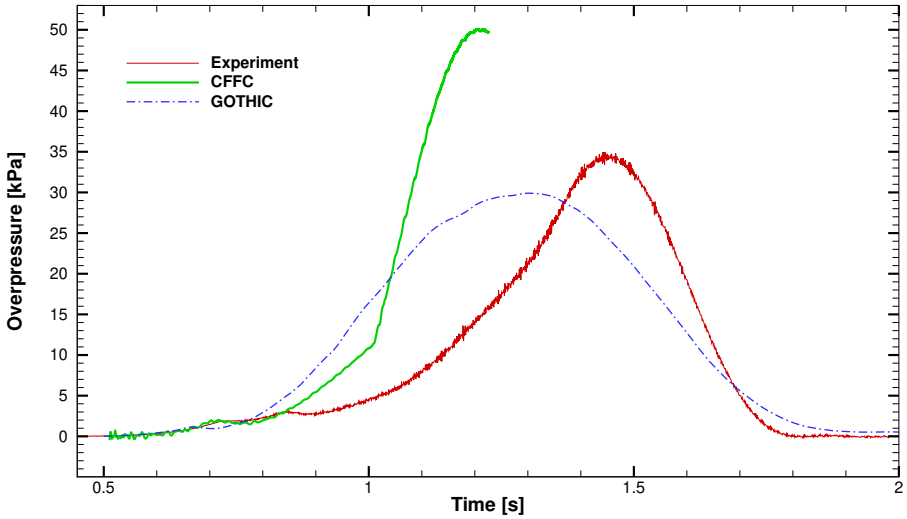

Figure 7: Predicted time histories of the vessel overpressure by the LP and LES models for the half-chamber case with 9% hydrogen fuel-air mixture and turbulent conditions. The pressure transients are compared to the LSVCTF measurements.

7.0 ACKNOWLEDGMENTS

The authors gratefully acknowledge the funding from the Atomic Energy of Canada Limited under the auspices of the New Technology Initiative Fund Program. Computational resources for performing all of the calculations reported herein were provided by an internal cluster facility at the Canadian Nuclear Laboratories and the SciNet High Performance Computing Consortium at the University of Toronto and Compute/Calcul Canada through funding from the Canada Foundation for Innovation and the Province of Ontario, Canada.

References

[1] R. K. Kumar, W. A. Dewit, and D. R. Greig. Vented explosion of hydrogen-air mixtures in a large volume. *Combustion Science and Technology*, 66:251–266, 1989.

[2] Z. Liang. Scaling effects of vented deflagrations for near lean flammability limit hydrogen-air mixtures in large scale rectangular volumes. *International Journal of Hydrogen Energy*, 42(10):7089–7103, 2017.

[3] Z. Liang. Vented deflagrations for near lean flammability limit hydrogen-air mixtures in large scale interconnected volumes. *Int. J. Hydrog. Energy*, 42(20):14321–14331, 2017.

[4] State-of-the art report on flame acceleration and deflagration-to-detonation transition in nuclear safety. Technical Report NEA/CSNI/R(2000)7, Nuclear Energy Agency, 2000.

[5] ISP-49 on hydrogen combustion. Technical Report NEA/CSNI/R(2011)9, Nuclear Energy Agency, 2012.

[6] V. Molkov, R. Dobashi, M. Suzuki, and T. Hirano. Modeling of vented hydrogen-air deflagrations and correlations for vent sizing. *Journal of Loss Prevention in the Process Industries*, 12(2):147–156, 1999.

[7] V. Molkov. *Fundamentals of hydrogen safety engineering II*. Ventus Publishing ApS, 2012.

[8] K. Voelsing. *GOTHIC Thermal Hydraulic Analysis Package Technical Manual Version 8.2 (QA)*. Electric Power Research Institute Inc., October 2016.

[9] R. Taylor, C.P.T. Groth, Z. Liang, and L. Ivan. Mesh-independent large-eddy simulation with anisotropic adaptive mesh refinement for hydrogen deflagration prediction in closed vessels. In *Proceedings of the 8th International Conference on Hydrogen Safety*, September 2019. Adelaide, Australia.

[10] I.C. Tolias, J.R. Stewart, A. Newton, J. Keenan, D. Makarov, J.R. Hoyes, V. Molkov, and A.G. Venetsanos. Numerical simulations of vented hydrogen deflagration in a medium-scale enclosure. *Journal of Loss Prevention in the Process Industries*, 52:125–139, 2018.

[11] I.C. Tolias and A.G. Venetsanos. An improved CFD model for vented deflagration simulations – analysis of a medium-scale hydrogen experiment. *International Journal of Hydrogen Energy*, 43(52):23568–23584, 2018.

[12] I.C. Tolias, A.G. Venetsanos, M. Kuznetsov, and S. Koutsoukos. Evaluation of an improved CFD model against nine vented deflagration experiments. *International Journal of Hydrogen Energy*, 46(23):12407–12419, 2021. ICHS 2019 Conference.

[13] L. Lebel and Z. Liang. GOTHIC simulations of OECD/NEA THAI multi-vessel hydrogen deflagration tests. *Annals of Nuclear Energy*, 150:107834, 2021.

[14] T. Kindred. *GOTHIC Thermal Hydraulic Analysis Package*. EPRI, version 8.3(QA) edition, November 2018.

[15] D.M. Solberg, J.A. Pappas, and E. Skramstad. Observations of flame instabilities in large scale vented gas explosions. *Symposium (International) on Combustion*, 18(1):1607–1614, 1981. Eighteenth Symposium (International) on Combustion.

[16] D.J. Rasbash, D.D. Drysdale, and N. Kemp. Design of an explosion relief systems for building handling liquefied fuel gases. In *Institution of Chemical Engineers Symposium Series*, volume 47, pages 145–156, 1976.

[17] S. Chippett. Modeling of vented deflagrations. *Combustion and Flame*, 55(2):127–140, 1984.

[18] F.E. Hernández-Pérez, F.T.C. Yuen, C.P.T. Groth, and Ö.L. Gülder. Les of a laboratory-scale turbulent premixed bunsen flame using fsd, pcm-fpi and thickened flame models. *Proceedings of the Combustion Institute*, 33(1):1365–1371, 2011.

[19] F.E. Hernández-Pérez, C.P.T. Groth, and Ö.L. Gülder. Large-eddy simulation of lean hydrogen–methane turbulent premixed flames in the methane-dominated regime. *International Journal of Hydrogen Energy*, 39(13):7147–7157, 2014.

[20] N. Shahbazian, M.M. Salehi, C.P.T. Groth, Ö.L. Gülder, and W.K. Bushe. Performance of conditional source-term estimation model for les of turbulent premixed flames in thin reaction zones regime. *Proceedings of the Combustion Institute*, 35(2):1367–1375, 2015.

[21] U. Piomelli, A. Rouhi, and B.J. Geurts. A grid-independent length scale for large-eddy simulations. *Journal of Fluid Mechanics*, 766:499–527, feb 2015.

[22] A. Rouhi, U. Piomelli, and B. J. Geurts. Dynamic subfilter-scale stress model for large-eddy simulations. *Physical Review Fluids*, 1(4):044401, aug 2016.

[23] V. Molkov and M. Bragin. Hydrogen–air deflagrations: Vent sizing correlation for low-strength equipment and buildings. *International Journal of Hydrogen Energy*, 40(2):1256–1266, 2015.

[24] D.G. Goodwin, R.L. Speth, H.K. Moffat, and B.W. Weber. Cantera: An object-oriented software toolkit for chemical kinetics, thermodynamics, and transport processes. `https://www.cantera.org`, 2021. Version 2.5.1.

[25] V.A. Alekseev, M. Christensen, and A.A. Konnov. The effect of temperature on the adiabatic burning velocities of diluted hydrogen flames: A kinetic study using an updated mechanism. *Combustion and Flame*, 162(5):1884–1898, 2015.

[26] B. van Leer. Towards the ultimate conservative difference scheme. v. a second-order sequel to Godunov's method. *Journal of Computational Physics*, 32:101–136, 1979.

[27] P. L. Roe. Approximate Riemann solvers, parameter vectors, and difference schemes. *Journal of Computational Physics*, 43:357–372, 1981.

[28] R. R. Rogallo. Numerical experiments in homogeneous turbulence. Technical report, NASA, 1981. Technical Memorandum 81315.